THE BELL SYSTEM TECHNICAL JOURNAL
Vol. 60, No. 4, April 1981
Printed in U.S.A.

Magnetic Localization of Buried Cable by the SCARAB Submersible

By S. H. FRANCIS, H. R. LUNDE, T. E. TALPEY, and G. A. REINOLD

(Manuscript received June 19, 1980)

A magnetometer array has been installed aboard the SCARAB submersible to enable it to detect and track buried undersea telephone cable. Four three-axis magnetometers sense the magnetic field of a 25-Hz current applied to the cable. The magnetometer signals are filtered, amplified, digitized, and multiplexed onto SCARAB's umbilical cable for transmission to the control ship. A shipborne minicomputer processes these signals in real time to determine the cable location, which is continuously displayed to SCARAB's operator on a graphics terminal. This paper describes the development and capabilities of the system. Among the topics discussed are a history of the cable-locating problem, an analysis of the factors governing the achievable 25-Hz signal level, a description of the magnetic noise spectrum and its sources, and a discussion of the signal-processing techniques. We also examine the dependence of system performance on signal and noise levels.

I. INTRODUCTION

SCARAB (Submersible Craft Assisting Repair and Burial) is a new class of unmanned cable-controlled submersible craft whose mission is to facilitate the maintenance of undersea telephone cable systems. The first SCARAB, now under development, is owned and will be operated by a consortium including AT&T Long Lines and British, Canadian, and French telecommunications companies.* A second SCARAB belongs to Transpacific Communications, Inc., a subsidiary of AT&T Long Lines. The SCARAB vehicle, shown in Fig. 1, is typical of other recently designed unmanned submersibles. The basic structural element is a

* Transpacific Communications, Inc. (a subsidiary of AT&T Long Lines); Cable and Wireless, Ltd.; French Postes Télégraphe et Téléphonie; British Post Office; Teleglobe Canada.

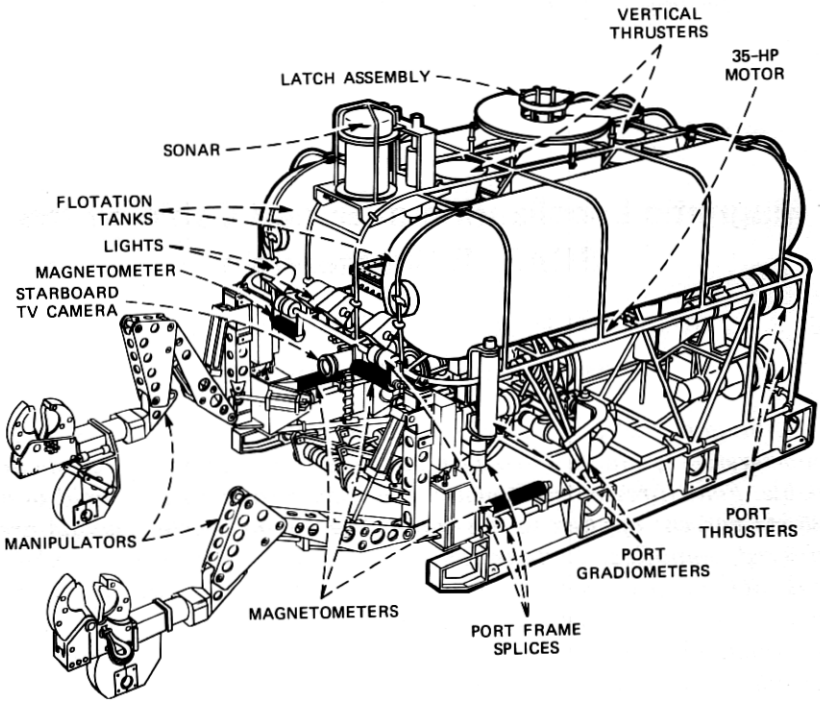

Fig. 1—SCARAB's major subsystems.

frame of welded aluminum rod. Flotation tanks are mounted on the frame to provide buoyancy, and seven thrusters are used for propulsion. Two of the thrusters are oriented vertically to allow the vehicle to dive and ascend. Two manipulators are provided for cutting and gripping cable. A water pump is used in conjunction with dredger and jetter attachments for unburying and burying cable. Additional equipment includes TV systems, acoustic devices, and a sensor system that includes the cable detection apparatus.

Operationally, SCARAB is designed to perform two specific functions: to assist during the repair of faulted cable, and to perform surveys of operational cables. During a repair operation, SCARAB magnetically locates the cable track and, subsequently, the point of the fault. It then unburies and cuts the cable as required, and attaches grippers so the cable ends can be lifted to the cable ship. Once both ends are aboard the ship, the cable is spliced, tested, and then lowered to the sea bed. The SCARAB then cuts away the lowering lines and reburies the exposed length of cable.

Basically, the survey operation is to follow the cable and measure the burial depth with the use of the magnetometer detection system.

If a point of shallow burial or cable exposure were detected, the vehicle would rebury using the jetter.

The purpose of the present paper is to describe in some detail SCARAB's cable-locating subsystem, designed and constructed by Bell Laboratories. More precisely, SCARAB has two distinct cable-locating systems, for reasons discussed below. The ac system described herein is considered the primary system; the dc system (not described) is intended to serve as a backup under certain operational circumstances.

II. HISTORY OF CABLE-LOCATING PROBLEM

Telephone cable systems use single coaxial cables whose outer diameters are between 2.5 and 5 cm, with repeaters inserted every 5 to 40 nautical miles, depending on the system. (The newer systems have the larger cable and closer repeater spacing.) Since the first transatlantic telephone cable was laid in 1956, the major threat to undersea cables has been the trawling and dredging operations of fishermen on the Atlantic continental shelves. In fact, about 95 percent of undersea telephone cable failures have been attributed to fishing activities. The principal response to this threat, aside from more heavily armoring the shelf sections of cables, was the development in 1966 of the first of a series of plows (Sea Plows I to IV) for burial of ocean cable.[1] Early versions of the sea plow buried the cable to a depth of 70 cm, leaving the repeaters exposed; the latest plow[2] buries the repeaters as well.

Burial reduces the likelihood of cable faults but by no means forestalls them. Even a buried cable system is vulnerable near unburied repeaters, or where cable burial was impeded by adverse bottom conditions, or where bottom erosion occurs after plowing, or where ships' anchors may drag.

This vulnerability, though minimized, nevertheless poses a problem: if a buried cable is damaged, how can it be found and its fault localized? An approximation to the fault location can be obtained from shore by combining knowledge of the cable's route with an estimate of the offshore distance to the fault, the latter obtained by any of several electronic fault-locating techniques applied at the cable's shore terminal. This procedure can identify the faulty repeater section, thereby isolating the fault to within a few miles, but the problem remains for the cable-repair ship to pinpoint the fault location and recover the cable. This problem is considerably exacerbated by burial of the cable, a fact recognized at the time the first sea plow became operational. To provide repair ships with the capability of finding buried cables, Bell Laboratories developed three varieties of electromagnetic probe: an electrode pair to be streamed behind the repair ship with a horizontal spacing of about 50 m; a 76-cm long magnetic induction coil to be

towed at low speeds in a vertical orientation near the sea floor; and a smaller induction coil for hand-held use by a diver.

To use the probes, a low-frequency signal (20 to 40 Hz) is applied between the cable's center conductor and ground at the shore cable terminal nearer the fault. This signal propagates along the cable, and its electric field can be detected at sea by the electrode system streamed behind the repair ship, allowing the ship to track the cable at relatively high speeds by zigzagging across it. Unless signal attenuation is excessive, the most seaward location at which the signal is detected provides a crude fault-location estimate, which can be refined by towing the induction coil at slow speeds so that it hangs nearly vertically, indicating by a null when it is above the cable. It was intended at this stage of the repair operation that a diver, using the hand-held probe to pinpoint the fault location, attach lifting lines and, if necessary, cut the cable. However, because of the depth limitations and inherent danger of diving operations, the usual procedure is to pick up the cable by grappling. Although grappling is quite straightforward for unburied cable, grappling has obvious disadvantages when applied to buried cable. The grapnel may not penetrate the bottom consistently to the cable's burial depth, thereby running the risk of missing the cable completely; or the cable may not have adequate tensile strength to withstand being pulled obliquely (often nearly horizontally) out of the bottom through more than a meter of mud or sand. These problems and similar ones motivated SCARAB's development.

III. CABLE LOCATING BY SCARAB: OPERATIONAL REQUIREMENTS AND SYSTEM CONCEPTS

3.1 SCARAB's cable-locating requirements

During a typical repair operation, SCARAB is called upon to find a buried cable and track it for possibly a mile or more until the cable fault is located. Thereupon it must position itself on the bottom, close to the cable, so its dredger and manipulators can be used to unbury the cable, cut it if necessary, and attach a lifting line. Cable reburial follows cable repair. SCARAB may also be required to estimate the cable's burial depth, both during repair operations and during survey of operational cable, to determine whether the cable should be buried more deeply.

In view of the complexity of these tasks and the difficulty of remotely maneuvering a swimming vehicle within a few meters of the bottom, the cable-locating system aboard SCARAB must be considerably more sophisticated than the ship-towed system described above. A principal limitation of the ship-towed system, from the viewpoint of its possible application aboard SCARAB (e.g., by mounting a single induction coil

on the vehicle), is its reliance on a single sensor, which measures only one component of the electric or magnetic field vector, and at only one point in space. Clearly, one instantaneous measurement of this kind is insufficient to localize the cable, which therefore can only be found by maneuvering the probe to a variety of positions near the cable (e.g., zigzagging), noting the field component as a function of time (and therefore of space), and using this time series to estimate the cable's location.

This procedure serves well where the information required concerning the cable's location is minimal and qualitative, such as during a grappling operation, where one usually needs only to know which of two opposite courses will cross the cable. However, for quantitative cable localization (e.g., to determine cable burial depth), this procedure would of course require real-time computer processing; but furthermore the processing algorithm would require knowledge of the vehicle's track over the bottom so that past history could be used to determine present cable location. Hence the computer would need accurate data concerning vehicle speed and ocean current; of these, the former is difficult to measure accurately at slow speeds and the latter is virtually impossible to measure from a swimming vehicle. (The problem is analogous to ship navigation using running fixes, a procedure whereby past and present lines of position are conjoined to determine the ship's position. The past line of position is updated using a dead-reckoned ship's track, which is subject to errors in the estimated course and speed of the ship and the set and drift of the current. The procedure is viable only because the ship's speed is usually large compared with the errors in its assumed speed over the bottom, and because the requirements for positional accuracy are not stringent. Neither of these helpful conditions pertains to SCARAB's cable-localization problem.)

So that estimates of track over the bottom do not have to be relied upon, a precision cable-locating system must have enough sensors so that their outputs, taken at a single instant of time, are sufficient to determine cable location without using any past data. For this purpose, a minimum of five sensors is required, since four parameters are needed to specify a given line in space (the cable location) and one parameter is needed to specify the cable current. In fact, for reasons discussed below, it proves convenient to use 12 sensors, packaged in four three-axis modules.

3.2 Choice of sensor

An attractive possibility for a cable-locating sensor is a bottom-penetrating sonar. In fact, a parametric sonar has succeeded in detecting telephone cable buried under 30 cm of sand in a laboratory tank experiment.[3] Although the feasibility of a sonar cable detector has

been thereby strongly suggested, the time and funding required to develop an operational sonar system for SCARAB were judged to exceed the available resources. Accordingly, attention was focussed on passive electromagnetic sensors.

The next choice to be made was between electric and magnetic sensors. Because at least five sensors would have to be mounted on a small vehicle crowded with other equipment, compactness was an overriding concern. From this viewpoint, electric sensors (i.e., electrode pairs) are a disadvantage because their size, determined by their baseline length, is normally considerably larger than a comparably sensitive magnetic detector. Furthermore, the technology of commercially available magnetic sensors is well advanced, having benefited from long-standing geophysical and military interest in compact and reliable magnetic detectors (an interest with no counterpart in electric-field detection). For these reasons, and because the geometry of the cable's magnetic field offers some processing advantages over its electric-field geometry, magnetic cable detection was chosen.

Magnetic detectors fall into three categories, according to the magnetic quantity measured: total-field magnetometers (measuring the field magnitude), component magnetometers (measuring individual vector field components), and induction coils (measuring the time derivative of individual field components).

Of these, induction coils can be readily dismissed from further consideration. Their sole advantage over magnetometers is their lower self-noise level, which is irrelevant in this application because other noise sources dominate self noise. Their principal disadvantages are the size and the weight of their cores (important considerations for a small equipment-laden vehicle that must be positively buoyant).

The choice between total-field and component magnetometers is not as straightforward. To clarify the functional difference between them, consider the case of a total-field magnetometer in the presence of the earth's field $\mathbf{B}_e$ and a cable field $\mathbf{B}_c$, where $|\mathbf{B}_c| \ll |\mathbf{B}_e|$ (as is always the case in practice). If $\hat{\mathbf{b}}$ is a unit vector parallel to $\mathbf{B}_e$, then the magnetometer output is $|\mathbf{B}_e + \mathbf{B}_c| \cong |\mathbf{B}_e| + \hat{\mathbf{b}} \cdot \mathbf{B}_c$, which is simply the component of the total field parallel to the earth's field (i.e., the perpendicular components of the cable field do not contribute). A total-field magnetometer is therefore completely equivalent to a component magnetometer oriented along the earth's field.

Suppose now that $\mathbf{B}_c$ is time-varying, so that its contribution to the magnetometer output can be separated from that of the earth's static field by filtering, leaving a signal of $\hat{\mathbf{b}} \cdot \mathbf{B}_c$ from the total-field device and $\hat{\mathbf{a}} \cdot \mathbf{B}_c$ from the component device (where $\hat{\mathbf{a}}$ is a unit vector parallel to the magnetometer axis). The sole distinction between these outputs is that $\hat{\mathbf{b}}$ is fixed while $\hat{\mathbf{a}}$ is changeable (i.e., a component magnetometer can be oriented to measure any desired component).

This flexibility of the component magnetometer is both an advantage and a disadvantage. The advantage is that three component magnetometers with mutually orthogonal axes can be combined in a single package to create a vector sensor (i.e., a sensor which detects all three components of the vector field). Because the electromagnetic field is a vector field, there are crucial signal-processing advantages to be gained by employing a vector sensor, as will be seen. The disadvantage of the component magnetometer is that it is subject to a potentially severe source of noise if mounted on a moving vehicle. As the vehicle maneuvers, pitches, and rolls, it changes the orientation of the magnetometer's axis relative to the earth's field, so that in the earth coordinate system $\hat{\mathbf{a}}$ is time-varying. The magnetometer output is therefore $[\mathbf{B}_c(t) + \mathbf{B}_e] \cdot \hat{\mathbf{a}}(t)$, and the contribution from the earth's field can no longer be removed by filtering unless $\hat{\mathbf{a}}(t)$ has negligible frequency components in the frequency band of the signal $\mathbf{B}_c(t)$. Because the earth's field normally exceeds the cable field by nearly four orders of magnitude, even slight vehicle motions can produce intolerable levels of motional noise if these motions are in the signal frequency band.

The choice between total-field and component magnetometers therefore hinges on whether a usable signal frequency exists, at which motional noise is acceptably small. As will be shown below, SCARAB has sufficient inertia and stability, so when it is submerged, motional noise is negligible at frequencies above a few Hertz. This fact was not known when the choice of sensor had to be made, because SCARAB had not yet been built; accordingly, an experiment was conducted using the Navy's CURV III, a cable-controlled underwater recovery vehicle quite similar in design to SCARAB. A component magnetometer mounted aboard CURV III revealed not only that motional noise was acceptably low at all frequencies of possible interest, but also that magnetic noise from all sources (notably the thrusters) was low enough to encourage the development of the cable-locating system described below.

3.3 Choice between ac and dc signals

A further preliminary question concerned whether the system should operate at ac or dc. An ac system would detect the ac magnetic field of a low-frequency current on the cable. A dc system would detect the superposition of dc fields from two sources: dc current on the cable, and permanent magnetization of the cable's steel components (central strength member or external armor wires).

The overriding difference between ac and dc cable detection derives from the existence of a large dc component of the earth's field. To detect the small dc cable field in the presence of the earth's field, one must use the fact that the earth's field is spatially homogeneous,

whereas the cable field is a localized anomaly. Therefore, to detect the cable one must detect differences between field values at different locations in space; if these values differ, the cable is nearby. This procedure can be implemented with one sensor by moving it in space and watching for changes in signal. Or it can be implemented with multiple sensors by looking at the differences among their signals. The first of these techniques must employ a total-field sensor, since a vector sensor would be subject to changes in orientation as it was moved (the dc equivalent of motional noise). The second of these techniques could employ either total-field or component sensors, though usually component sensors are used, with two being packaged in the same housing to maintain their parallelism. Such a configuration is termed a gradiometer, since its output is proportional to the field gradient if the sensor separation is small.

One contrast between ac and dc cable detection, therefore, is in the type of sensor that can be used: ac detection can use a vector magnetometer, while dc detection requires a total-field magnetometer or gradiometer. Put another way, the ac sensor measures a vector quantity while the dc sensor measures either a scalar or a tensor quantity. Because the magnetic field is a vector, one might expect the vector sensor to lend itself more readily to data processing for cable localization, thereby favoring ac over dc. In fact, this expectation is borne out: the ac cable-locating algorithm described below is extremely simple, whereas a comparable dc algorithm has not yet been devised.

Nonetheless, a dc cable-locating system possesses certain advantages over ac. Since undersea telephone cables normally carry a dc current (with sea return) to power the repeaters, a dc detection system does not require a special signal to be placed on the cable, and the system works as well for an operational cable as for a broken cable. Furthermore, unlike an ac signal, the dc current does not diminish exponentially with distance from shore, so both ends of a broken cable can be powered with comparable current levels. In fact, when the cable is armored it does not need to be powered at all for dc detection, which can take advantage of the relatively large fields of the steel armor wires. In contrast, an ac signal cannot propagate across the ocean, and therefore, at best, it can reach only one side of a break in a transoceanic cable. Under certain circumstances, therefore, the unique capabilities of a dc system may be necessary.

In sum, dc sensors provide magnetic data of a type that is not suitable for cable localization, with the result that an ac system is normally preferable. However, operational circumstances exist for which an ac system would be ineffective and a backup system is desirable. For these reasons, a dc system is under development for SCARAB to supplement the ac system.

The remainder of this paper describes the implementation and operational performance of the ac system.

3.4 Cable-localization algorithm and array design

In the preceding sections we proposed that the optimum cable-locating system should employ a vector sensor (i.e., a sensor detecting all three field components), because in some sense a vector sensor is better suited to characterizing a vector field. A corollary was that the optimum system was an ac system, to avoid the earth's dc field. A further proposition was that the optimum system should have enough sensors to determine cable location instantaneously, without having to rely on past history.

To particularize these general considerations, this section describes the method implemented aboard SCARAB for instantaneous cable localization by a number of ac vector sensors. The method relies on the fact that the magnetic field lines caused by the cable's current are circles (assuming the cable lies in a straight line). This geometry permits cable localization by a simple triangulation procedure most easily visualized in two dimensions (Fig. 2). Vector sensors are used to determine the direction of the field at two locations. At both locations a line perpendicular to the field is constructed. Because these two lines lie along radii of concentric circles, their point of intersection is the common center: the cable location. The generalization of this procedure to three dimensions is straightforward: at two locations, construct planes perpendicular to the field direction, and determine the line at which these planes intersect. This line of intersection is the cable's location.

In principle, this procedure allows cable localization with only two

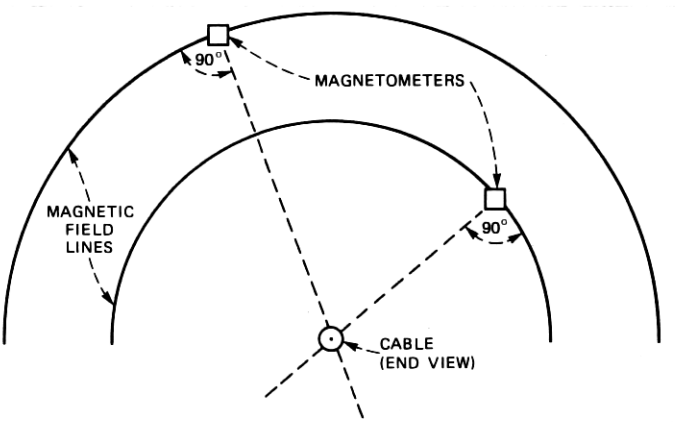

Fig. 2—Cable location in two dimensions. SCARAB's computer employs a three-dimensional generalization of this principle.

vector magnetometers. Moreover, even this basic system overdetermines the problem: a line in space can be described with four parameters, whereas two vector sensors provide six scalar measurements. These six measurements can be manipulated to provide information on field direction (four angles) and size (two magnitudes). Cable localization requires only the four angles; the two magnitudes can provide two cable-current estimates, which would of course coincide in the absence of noise and other sources of field distortion.

However, this simple system of two vector sensors must be embellished, for it fails when the two sensors and the cable all lie in the same plane (or, in the presence of noise, nearly in the same plane). This degenerate case cannot be ignored, for it occurs quite commonly for any two-sensor array. For example, to optimize cable tracking it would be logical to place the two sensors symmetrically to port and starboard, so that the sensors straddle the cable when SCARAB does. For such a placement, however, SCARAB would be unable to do cable localization while heading perpendicular to the cable, such as during initial cable acquisition.

The solution is to provide more than two sensors, and to implement a procedure for deciding which sensors shall be used and which ignored. To ensure that no cable location shall be coplanar with all pairs of sensors, a nonplanar array of at least four sensors is required.

The optimum position of these four sensors is governed by the desire that the planes whose intersection determines cable location should intersect nearly at right angles, since then the cable-location errors caused by noise-induced fluctuations of these planes will be minimized. For right-angle intersection, the baseline length between two sensors must be twice the distance from the baseline to the cable. However, SCARAB's maximum baseline length is constrained to be less than two meters (since booms extending beyond the vehicle's perimeter are undesirable), while SCARAB's height above the sea floor will generally be at least one meter. Consequently, right-angle triangulation is impossible to achieve, and the effects of noise are minimized simply by spacing the sensors as far apart as possible, maximizing the distance between each sensor and the plane defined by the other three. In fact, even this modest goal is impractical, because most potential sensor sites in the center and after parts of the vehicle are contaminated by thruster noise and frame-current distortion of the magnetic field (see below). Consequently, the best available array configuration comprises four coplanar sensors in a nearly vertical plane in the forepart of the vehicle (Fig. 1). This array is not well suited to localizing a cable which lies athwartships and underfoot (i.e., a cable in the plane of the sensors), but for all other cable locations it serves well.

Such an array of four sensors provides six possible sensor pairs and therefore six cable-location estimates, if the outputs from all pairs are

used. Since some pairs will be better situated than others to triangulate the cable, a choice must be made among them. This choice is made by calculating a weighted average of the six cable-location estimates, which de-emphasizes sensor pairs whose measured magnetic fields are nearly parallel. The weighting function used is $\sin \theta$,[4] where θ is the angle between the magnetic fields and therefore between the planes whose line of intersection is sought. This weighting function satisfies the requirement that it increase monotonically from 0 at $\theta = 0°$ (the most undesirable case) to 1 at $\theta = 90°$ (the most desirable case), but beyond this requirement its choice is rather arbitrary.

This section has described how SCARAB's ac cable-location system works, in principle. Outputs from an array of four vector magnetometers are combined in a shipboard computer, using a rather simple cable-locating algorithm and weighting scheme, and the resulting estimate of cable location is displayed to SCARAB's operator so that he may maneuver the vehicle accordingly. How well this sytem works in practice depends on the relative levels of signals and noise. This is addressed in Section IV.

IV. SIGNAL AND NOISE

4.1 Signal

The magnetic field **H** of a line current I in an infinite homogeneous nonconducting medium satisfies

$$|\mathbf{H}| = \frac{I}{2\pi\rho}, \tag{1}$$

where **H** is in amperes/meter, I is in amperes, and ρ is the distance from the line current in meters. In a conducting medium such as sea water, this expression is valid only if $\rho \ll \delta$, where δ is the skin depth. In sea water, however, $\delta \cong 250/f^{1/2}$ meters, where f is the frequency in hertz, so that $\delta > 40$ m for all frequencies less than 40 Hz. Equation (1) is therefore well satisfied within about 20 m of the cable. This conclusion is unaffected by the presence of the sea bottom, whose lower conductivity causes no appreciable field distortions except at distances greater than a sea-water skin depth. An important implication is that the circular geometry of the field lines, on which SCARAB's cable-location method relies, is not appreciably distorted by the presence of the sea bottom except at ranges in excess of 20 m.

To characterize the signal, therefore, it remains only to specify I, the net current on the cable. When a signal current is fed to the center conductor at the shore terminal, return currents flow partially in the sea and partially in the outer conductor, metallic shielding tapes, and armor wires, if any. The net current I, which determines the field according to eq. (1), is the algebraic sum of all currents on the cable's

various conductors. This net current attenuates as the signal propagates seaward, because of losses in the cable, the sea water, and the repeaters (which introduce loss rather than gain because the low-frequency signal follows the dc power path through the repeaters rather than the path through the carrier-frequency amplifiers). For example, Fig. 3 shows a theoretical prediction of propagation at several frequencies along a 100-mile section of armored cable with 5-mile repeater spacing and with a cable break at the offshore end. The appendix describes the theory underlying Fig. 3. The net current is lower at higher frequencies, not only because the losses are greater, but also because the outer conductor carries a greater share of the return current (so that the net current, being the algebraic sum of center- and outer-conductor currents, is less). Clearly, from the viewpoint of signal propagation, we prefer the lower frequencies.

The choice of operating frequency, however, is ideally based on maximizing the signal-to-noise ratio. This ideal requires knowledge of the vehicle's noise spectrum, however, and SCARAB's development schedule did not permit delaying the choice of frequency until the vehicle was completed and its noise spectrum measured. Therefore, we provisionally chose 25 Hz for convenience, since 25 Hz is a frequency commonly used with ship-towed probes (though its choice in that context was influenced by considerations entirely irrelevant to SCARAB, such as the low-frequency falloff of induction-coil sensitivity and the expected low-frequency noise caused by turbulence-induced motion of

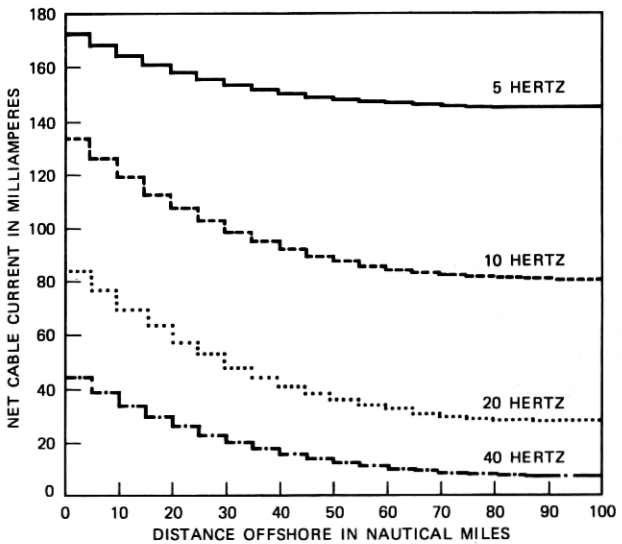

Fig. 3—Propagation of low-frequency signals on armored SG cable with a cable break 100 nmi offshore. The center-conductor current is 200 mA at the shore point, for all frequencies. The step discontinuities occur at the repeaters, which are unpowered.

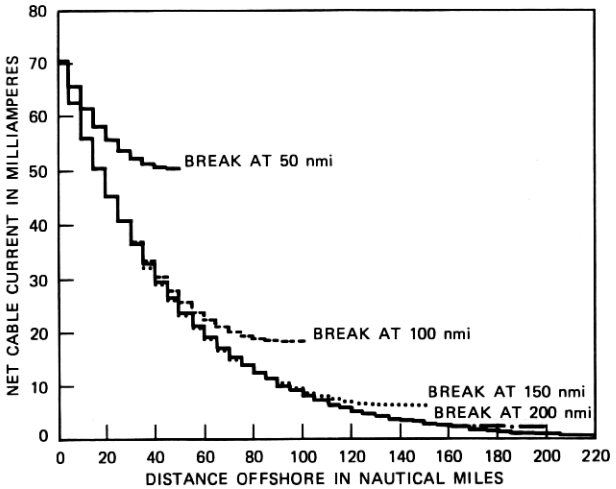

Fig. 4—Propagation at 25 Hz on armored SG cable with cable breaks at various locations. The unlabeled curve extending to 220 nmi is for an unbroken cable. The center-conductor current at the shore point is 200 mA (but note that the vertical scale extends only to 80 mA). The step discontinuities occur at the repeaters, which are unpowered.

a ship-towed coil). Although the choice of 25 Hz was therefore arbitrary to some degree, subsequent determination of SCARAB's noise spectrum (Section 4.2) showed that 25 Hz lies in a rather quiet region of the spectrum, and so we have retained it as SCARAB's operating frequency.

Figure 4 illustrates propagation at 25 Hz on the same type of cable system as Fig. 3, but with cable breaks at various distances offshore. Notice that a cable break enhances the signal by total reflection of the propagating mode, thereby roughly doubling the cable current at the fault relative to the current on an intact cable. A broken cable is therefore twice as easy to detect as an intact one (if both carry the same current at their shore points).

Aside from the question of signal attenuation, the maximum current that can be propagated to the desired detection point is restricted by the maximum center-conductor current tolerated by the repeaters. This value is 100 or 200 mA (rms), depending on the cable system, except when the system is operational, in which case no more than 20 mA (rms) can be tolerated without affecting service. Broken cables therefore can carry at least ten times the signal of operational cables, with a factor of at least five due to the higher allowed current and a factor of two due to the signal reflected from the cable break.

4.2 Noise

Knowledge of the noise field and its sources is a prerequisite to predictions of operational performance, and also may suggest methods

of performance improvement. SCARAB's magnetic noise originates from a variety of sources, described below in rough order of decreasing importance.

4.2.1 Thruster noise

SCARAB's propulsion is by thrusters comprising induction motors (2300 volt, four pole, three phase, 60 Hz) driving shrouded screws. Six 5-hp thrusters are used, four for fore-and-aft propulsion and two for vertical propulsion (Fig. 1). A seventh thruster, horizonally oriented athwartships, is powered by the hydraulic system, whose pump is driven by a 35-hp motor. The noise spectra of CURV's and SCARAB's thrusters were measured in tank tests and, as would be expected for any rotating machinery, consisted of spectral lines with no measurable broadband component.

The basic frequencies of an induction motor's operation are the shaft-rotation frequency and the synchronous frequency (i.e., the apparent rotation rate of the stator's magnetic field). For a thruster with no external load or internal friction, these frequencies are the same, equalling the power frequency (60 Hz) divided by the number of pole pairs (two for SCARAB, three for CURV). Under load the thruster slows down, reducing the shaft-rotation frequency by an amount which, when multiplied by the number of pole pairs, is called the slip frequency. For example, the synchronous frequency of the SCARAB's thrusters is 30 Hz, while the shaft and slip frequencies at one-third speed are 10 Hz and 40 Hz, respectively.

Thruster noise is principally at four frequencies: the slip and shaft frequencies, and their sum and difference frequencies. Noise at higher harmonics, although measurable at high speeds, is small. The geometry of the noise field at the slip and shaft frequencies is consistent with an oscillating dipole source aligned parallel to the thruster axis. In contrast, the geometry of the noise field at the sum and difference frequencies is consistent with an oscillating and rotating dipole source aligned perpendicular to the thruster axis. By far the strongest of these lines is the slip-frequency line. As the speed of SCARAB's thrusters varies between zero and 90 percent speed (the maximum attainable under load), the frequency of this line varies between 60 Hz and 6 Hz, and its root-mean-square amplitude (expressed as an effective source dipole moment) varies between 0 and 19.6 γ-m^3 (where 1 $\gamma = 1/400\ \pi$ amp/m). The amplitude is roughly a linear function of the voltage, and therefore varies quite nonlinearly with motor speed (at half speed, the noise amplitude is about one quarter of its full-speed value).

The precise origin of these noise components is obscure, related in some way to secondary leakage fields and therefore to subtle details of motor design and manufacture. An illustration of the subtlety is that

a 5-hp SCARAB thruster has about six times the noise of a 10-hp CURV thruster when both are operated at maximum speed.

Thruster noise poses a potentially awkward problem, for it is composed of several spectral lines whose frequencies can attain any value between 0 and more than 60 Hz, depending on the operating speed. If the signal frequency were chosen higher than any attainable by thruster noise, a heavy penalty would be paid in the attenuation of the signal in its propagation from shore (Fig. 3). The alternative is to base the choice of frequency on other considerations and rely on being able to avoid thruster speeds producing excessive noise at the chosen frequency. The strongest constraint is on the use of the forward vertical thruster, which is closest to the magnetometer array. The operator must therefore be particularly careful in the use of that thruster while the cable-localization system is being used. In fact, during normal search and tracking operations the operator customarily relinquishes control of the vertical thrusters to SCARAB's automatic altitude control system, which servo-controls these thrusters to maintain the desired height above the bottom. Fortunately, this automatic altitude control system uses the vertical thrusters in a manner quite favorable to the cable-localization system.

To illustrate the effects of thruster noise, Fig. 5 shows a noise spectrum recorded using a three-axis magnetometer mounted on SCARAB at a point midway between the two upper magnetometers shown in Fig. 1. This point is well within a meter of the forward vertical thruster, is about 1.5 m from the 35-hp hydraulic-pump motor, and is more than 2 m from the thrusters at the stern. The spectrum was recorded during dockside tests in San Diego harbor, while SCARAB was swimming submerged at nearly full speed with the vertical thrusters controlled by the automatic altitude system. We feel that this spectrum is reasonably characteristic of the typical noise environment of all SCARAB's magnetometers.

In Fig. 5, the intense spectral line near 40 Hz comes from the forward vertical thruster, whose proximity to the magnetometer causes it to dominate the other noise sources. At the time the spectrum was taken, this thruster was operating at one-third speed, generating noise at its slip frequency near 40 Hz and at its sum frequency (i.e., shaft frequency plus slip frequency) near 50 Hz. These values of the frequency reflect typical operating speeds of the vertical thrusters, whose average speed in level flight is, of course, a direct function of the vehicle's buoyancy. The automatic altitude system maintains level flight using rather small speed excursions, in contrast with manual altitude control in which the natural tendency of the operator is to overreact by using large changes in vertical thrust.

In comparing the three components of the 40-Hz line, note that the

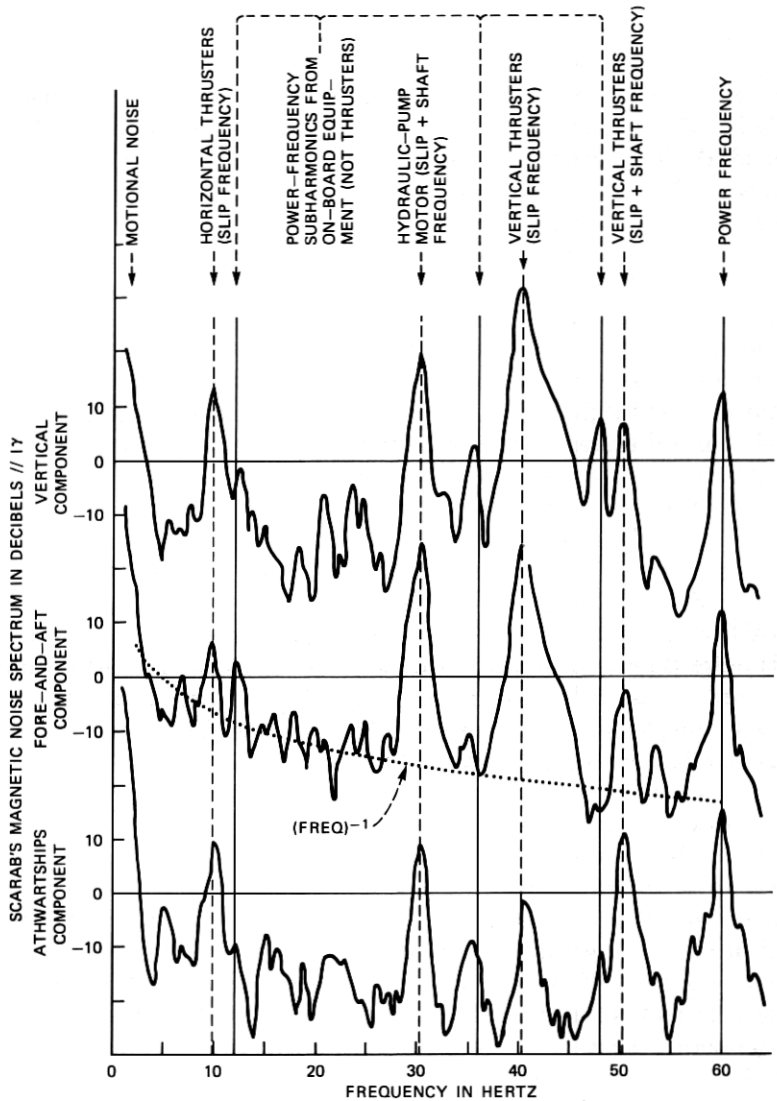

Fig. 5—Noise spectrum of vector magnetic field measured aboard SCARAB.

smallness of the athwartships component (relative to the other two components) is consistent with the tank-test result that the slip-frequency noise source is equivalent to a dipole parallel to the thruster axis.

Other spectral lines in Fig. 5 come from the horizontal thrusters and the hydraulic-pump motor. The horizontal thrusters, operating at nearly full speed, contribute noise at their slip frequency of about 10 Hz. Although they are generating more noise than the vertical thrusters (because of their higher speed and their greater numbers), their impact on the noise spectrum is substantially smaller because of their greater distance from the magnetometer.

The 35-hp hydraulic-pump motor operates at a constant speed just below its synchronous speed of 30 Hz, and its most important contribution to the noise spectrum is a strong line at its sum frequency (slip plus shaft frequency) just above 30 Hz. Its slip frequency is very low (near 1 Hz), and so its slip-frequency noise is of no practical importance.

From the spectrum in Fig. 5 it is clear that 25 Hz is a fortuitous choice of operating frequency, since it avoids the frequencies at which thruster noise is most severe. The frequencies of the horizontal and vertical thrusters are variable, of course, but it is quite practical to avoid the critical speed (58 percent) at which their slip frequency is 25 Hz. The vertical-thruster speed necessary to maintain level flight is substantially less than 50 percent at the vehicle's buoyancy, and the automatic altitude system maintains vehicle altitude without approaching the critical speed of 58 percent. On the other hand, we can expect the speed of the horizontal thrusters to pass through 58 percent in normal operation, but their noise level at this speed is substantially lower (by 8 dB) than their level in Fig. 5. As long as SCARAB does not swim continuously at this speed, the effects of the horizontal thrusters should be confined to small, short transients seen by the magnetometers each time the critical speed is passed.

In addition to the spectral lines discussed above, the spectrum of Fig. 5 contains noise at the power frequency and several other fixed frequencies. The 60-Hz line contains contributions from all the vehicle's equipment, but the predominant sources are the thrusters and the pump motor, since they draw the most current. Subharmonics of the power frequency at multiples of 12 Hz are also present, caused by unidentified equipment on board the vehicle other than the thrusters and pump motor. The subharmonic at 24 Hz is the weakest of these lines (not even showing on Fig. 5), and so its proximity to the 25-Hz operating frequency has no ill effects.

4.2.2 Frame currents

To continue the discussion of noise sources, this section describes the problem of distortion of the cable's field by currents induced in

SCARAB's structure. This type of noise is particularly insidious because of its perfect correlation with the signal. Although eddy currents in SCARAB's massive metal objects (such as the manipulator arms and flotation tanks) were found to have negligible effect, currents circulating in the supporting framework created a severe problem which had to be faced.

SCARAB is constructed as a welded framework of solid aluminum rods which support its flotation tanks, thrusters, sensors, and other equipment (see Fig. 1). The framework itself can be considered a passive electrical circuit which, because of the large cross section and high conductivity of the aluminum rods, has an extremely low impedance. This low impedance has an unfortunate consequence. Time-varying magnetic fields, inducing electromotive forces in the framework in accordance with Faraday's law, drive sizable currents in the frame members. These frame currents in turn cause secondary magnetic fields which, superposed on the primary fields, have the effect of distorting the field geometry on which the cable-locating system relies.

To appreciate the severity of this effect, consider a simplified framework in the form of a 1-m square composed of solid aluminum rods of 4-cm diameter (the size of SCARAB's main frame members). The calculated resistance of such a frame is 100 $\mu\Omega$ and its inductive reactance is $17f\ \mu\Omega$ (where f is the frequency in Hz). These calculations neglect the resistance of the welds and assume a frequency sufficiently low so that the skin effect is negligible (not quite true at 25 Hz, but nearly so). At frequencies above 6 Hz the framework is primarily inductive, at lower frequencies it is primarily resistive.

Now suppose that an infinite straight wire carries a sinusoidal current, situated in the same plane as the square frame but 1 m away and parallel to one edge. A straightforward application of Faraday's and Ohm's laws shows that for frequencies at which the framework's impedance is inductive (i.e., above 6 Hz), the induced frame current is about 5 percent of the primary current. Since a magnetometer mounted on the framework could easily be 20 times closer to the frame than to the wire, the secondary magnetic field seen by the magnetometer could easily rival the primary field in magnitude.

Although SCARAB's framework is topologically more complicated, the same effect is present. To estimate its impact, we ran tests in which a current-carrying wire was placed at various locations within a meter of the vehicle, and measurements were made of the magnetic fields (primary plus secondary) and of the currents flowing in the frame members. The amplitudes of the frame currents, measured with a specially modified clamp-on ammeter, were of the same order of magnitude as predicted in the preceding paragraph. Consequently, the field anomaly was large enough to defeat the cable-locating algorithm.

We contemplated three possible solutions to the problem. One thought was to reduce the operating frequency, thereby reducing the induced EMF proportionately. This solution would require lowering the frequency to 1 Hz or below, however, because at frequencies above a few hertz the impedance is inductive and therefore decreases along with the EMF as the frequency is decreased, so that the currents remain the same. Since frequencies at or below 1 Hz are objectionable for many reasons (e.g., motional noise), we discarded this alternative. Another thought was to mount the magnetometers far away from any frame members, thereby reducing the adverse effects of the frame currents. In practice, this alternative requires four booms that hold the magnetometers one or two meters outside the vehicle's perimeter and retract to prevent damage during vehicle launch or recovery. We did not attempt to implement such a system, although it is probably feasible, because a simpler alternative was available.

The final solution was to prevent the frame currents from flowing in critical frame members by cutting these members and splicing them back together with insulating splices. Obvious choices for splicing were the four frame members on which the four magnetometers are mounted. Also spliced were the two vertical frame members at the front of the vehicle (see Fig. 1). Frame currents flow in the remaining frame members, of course, but their distance from the magnetometers reduces the adverse effects to acceptable levels.

The combination of frame currents and thruster noise constrains the placement of magnetometers to the front of the vehicle, where there are no thrusters and where the density of frame members has been minimized to improve TV visibility. Initial plans included the placement of one magnetometer further aft, but the high density of frame members at the intended location (each of which would have had to be cut and spliced) forced the relocation of this magnetometer to the front of the vehicle. The consequence, as mentioned in a preceding section, is that the cable-localization system is blind to a cable which lies under the vehicle and perpendicular to its center line, but this blind spot does not significantly reduce the usefulness of the system.

4.2.3 Motional noise

The strong source of noise evident below 5 Hz in Fig. 5 is motional noise, attributable to changes in magnetometer orientation relative to the earth's magnetic field as SCARAB pitches, rolls, and yaws. The identification of this noise is verified by its absence when SCARAB is on a stable platform (such as the sea bottom). When SCARAB is surfaced in a seaway, a spectral peak in the motional noise at the frequency of the surface water waves is sometimes identifiable. Above 5 Hz, however, motional noise is negligible relative to other noise sources.

4.2.4 Broadband noise

In addition to narrowband noise from the sources described above, SCARAB's noise spectrum includes broadband noise which falls off with increasing frequency roughly as $1/f$ (see Fig. 5). This frequency dependence matches the Fourier transform of a step function, and indeed if one looks at the noise in the time domain (restricting attention to a quiet frequency band such as the neighborhood of 25 Hz), one sees a series of impulsive transients. This behavior suggests that the broadband noise is due to the combined effects of a number of weak, random, impulsive sources.

One example of such an impulsive source is the actuation of a solenoid, of which many are used in SCARAB's hydraulic system. In fact, under quiet circumstances the actuation of SCARAB's solenoids is readily observable by a magnetometer more than 2 m away. Other potential impulsive noise sources include any movable equipment with residual magnetization, such as SCARAB's manipulator arms and 35-mm camera (whose casing is highly magnetized, causing large broadband transients during panning and tilting). Slight random shifts in the position of such equipment would cause broadband noise of the kind observed.

Although the identification of the principal broadband sources remains speculative, there are a number of sources which can definitely be excluded from consideration, since their levels are demonstrably insufficient to account for the observed broadband levels. These sources include detector noise (generated within the magnetometer core), atmospheric noise (from nearby man-made sources or from worldwide thunderstorm activity, ducted by the ionosphere), and tape noise (on the magnetic tape used for recording test data).

4.3 Signal-to-noise ratio and cable-localization performance

With the signal and noise levels known, the performance of the cable-locating system can be predicted. Consider a typical scenario in which SCARAB is looking for a cable break 100 miles offshore. Figure 4 shows that the net current at the break is about 40 mA (rms) and Fig. 5 implies that the noise level in a 1-Hz band at 25 Hz is roughly $\frac{1}{4}\gamma$ (rms). The range at which the cable's signal, given by eq. (1), equals the noise level is 32 m, which may be termed the "cable-detection range."

At this range, however, and even well inside it, the cable-localization algorithm still does not have adequate signal-to-noise ratio to localize the cable because it is the field differences (rather than the fields themselves) that contain the significant information for localization. Therefore, to calculate a "cable-localization range" by equating signal and noise, one should use as the signal the field difference $\Delta H =$

$(\Delta\rho)(\partial H/\partial\rho)$, where $\Delta\rho$ is a measure of the mutual separation of SCARAB's sensors. To allow for the noise contributions (assumed to be correlated) from two magnetometers, the noise level should be increased by a factor of two. With $\Delta\rho = 1$ m, this calculation gives a localization range of 4 m.

As SCARAB approaches the cable, therefore, it passes through three regions in which it can infer increasing levels of information concerning the cable. Outside the detection range, it does not sense the cable. Inside the detection range but outside the localization range, it detects the proximity of the cable but has insufficient information to determine the cable's location. Inside the localization range it can localize the cable, with the precision of this localization increasing as the distance to the cable decreases. For a net cable current $I = 40$ mA (rms), the detection and localization ranges are 32 m and 4 m, and for other values of I they scale as I and $I^{1/2}$, respectively.

Localization of the cable is reasonably precise only at quite modest ranges (a few meters or less). The fundamental obstacle to localization at greater ranges is SCARAB's compactness, which imposes severe constraints on the size of the magnetometer array. However, the description in Section VI of SCARAB's operational use shows that the present localization range is quite adequate.

V. CABLE-LOCATING SYSTEM: DETAILS OF DATA COLLECTION, PROCESSING, AND DISPLAY

Preceding sections have discussed the cable-locating system in rather general terms, omitting details of the actual hardware and software which carry out the functions of data collection, processing, and display. Some of these specifics will now be discussed, to promote a better understanding of how the system works in practice.

5.1 Data collection

The sensors are four commercial three-axis ring-core fluxgate magnetometers. Each magnetometer is mounted in a cylindrical aluminum pressure housing with three preamplifiers whose function is to remove from the magnetometer outputs the dc components (which are proportional to the three components of the earth's dc field) and to amplify the residuals for transmission to an electronics housing at the stern of the vehicle. The relative gain among the three preamplifiers is adjusted to compensate for the differential attenuation of the magnetic field components by the cylindrical aluminum container (whose eddy currents reduce the 25-Hz field inside to about 82 percent of its outside value, with slight attenuation differences between the axial component and the other two).

Each magnetometer signal is then passed through a bandpass filter

at 25 Hz and band-elimination filters at 30 Hz and 60 Hz (to eliminate the pump-motor and power-frequency noise). The signals are then fed to rms detectors whose outputs are sampled five times per second, digitized by a 12-bit analog-to-digital converter, and multiplexed onto SCARAB's umbilical cable for transmission to a minicomputer on the control ship.

In addition to the rms amplitudes, the cable-localization algorithm requires the relative phases of the three field components from each magnetometer to allow determination of the orientation of the vector magnetic field. These relative phases (which are either 0° or 180°) are continuously determined by phase comparators whose outputs, sampled five times per second, are digitally coded and packed with the digitized amplitudes for transmission to the surface minicomputer.

The process of digitizing the amplitudes introduces a certain amount of error because of the uncertainty in the digitizer's least-significant bit and because of bias and fluctuations in its reference voltage. This error normally affects only the two lowest-order bits, and is equivalent to magnetic noise of about 0.1 to 0.2 γ (rms), somewhat less than (but not negligible compared with) the vehicle noise at 25 Hz. This digital noise level could be reduced by increasing the preamplifier gain, with the penalty that the digitizer, which presently saturates at fields of about 120 γ (rms), would saturate at proportionately lower levels. The present gain setting was predicated on keeping the effects of digital noise below those of vehicle noise while maximizing the field at saturation. It follows that any future improvement or degradation in vehicle noise may require corresponding gain changes to maintain the desired relationship between digital noise and vehicle noise.

5.2 Data processing

The data collection system just described provides the shipboard minicomputer with three field-component amplitudes and their relative phases from each of four magnetometers. Sensors on the vehicle also provide its digitized heading, pitch, roll, and height above the bottom. New data are provided five times per second.

The first step in the real-time processing of these data, after the relative phases are used to assign signs to the rms component amplitudes, is to calculate a time average of the magnetic fields using an exponentially decaying weight function,

$$\langle \mathbf{H} \rangle = \int_0^\infty \frac{dt}{\tau} e^{-t/\tau} \mathbf{H}(-t), \tag{2}$$

where τ is an averaging time and $\mathbf{H}(-t)$ denotes the magnetic field at a time t in the past. This running average, whose purpose is to reduce the effects of the noise, is updated with each new input of data (five

times per second). The value of τ is chosen by SCARAB's operator, and may be changed at will as dictated by the operational situation. The rationale for particular choices of τ will be discussed below.

Note that this averaging is not the only averaging undergone by the data. The 25-Hz bandpass filter (whose $Q = 20$) has the side effect of averaging the analog signals according to eq. (2) with $\tau = 0.25$ s.

From these averaged data the computer determines cable location twice per second according to the algorithm described geometrically in Section 3.4. To express the algorithm mathematically, let the cable location be specified by the vectors $\mathbf{r}_0$ and $\hat{\mathbf{a}}$, where $\mathbf{r}_0$ is the vector from the coordinate origin to the closest point on the cable and $\hat{\mathbf{a}}$ is a unit vector parallel to the cable. If the cable carries a net current I, then the magnetic field observed at any point $\mathbf{r}$ is

$$\mathbf{H}(\mathbf{r}) = \frac{I}{2\pi} \frac{\hat{\mathbf{a}} \times (\mathbf{r} - \mathbf{r}_0)}{|\mathbf{r} - \mathbf{r}_0 - \hat{\mathbf{a}}\hat{\mathbf{a}} \cdot (\mathbf{r} - \mathbf{r}_0)|^2}. \tag{3}$$

This equation is the vector generalization of the scalar eq. (1).

The core of the data-processing problem is to calculate the cable's location (expressed by $\mathbf{r}_0$ and $\hat{\mathbf{a}}$) from two measurements of the magnetic field ($\mathbf{H}_m$ and $\mathbf{H}_n$) made by two magnetometers located at coordinates $\mathbf{r}_m$ and $\mathbf{r}_n$. The dependence of $\mathbf{r}_0$ and $\hat{\mathbf{a}}$ on the measured parameters $\mathbf{H}_m$, $\mathbf{H}_n$, $\mathbf{r}_m$, and $\mathbf{r}_n$ is given by the two equations below, whose derivation follows:

$$\begin{aligned} \mathbf{r}_0 = {} & \frac{\mathbf{r}_m \cdot \mathbf{H}_m H_n^2 - \mathbf{r}_n \cdot \mathbf{H}_n \mathbf{H}_m \cdot \mathbf{H}_n}{H_m^2 H_n^2 - (\mathbf{H}_m \cdot \mathbf{H}_n)^2} \mathbf{H}_m \\ & + \frac{\mathbf{r}_n \cdot \mathbf{H}_n H_m^2 - \mathbf{r}_m \cdot \mathbf{H}_m \mathbf{H}_m \cdot \mathbf{H}_n}{H_m^2 H_n^2 - (\mathbf{H}_m \cdot \mathbf{H}_n)^2} \mathbf{H}_n, \end{aligned} \tag{4}$$

$$\hat{\mathbf{a}} = \frac{\mathbf{H}_m \times \mathbf{H}_n}{|\mathbf{H}_m \times \mathbf{H}_n|}. \tag{5}$$

These equations can be derived using mathematical arguments that parallel the geometrical discussion of Section 3.4. For variety, however, we present a more formal derivation.

Suppose for the moment that $\mathbf{H}_m$ and $\mathbf{H}_n$ are not parallel, in which case it is clear that the three vectors $\mathbf{H}_m$, $\mathbf{H}_n$, and $\mathbf{H}_m \times \mathbf{H}_n$ comprise a basis spanning three-dimensional vector space. The vectors $\mathbf{r}_0$ and $\hat{\mathbf{a}}$ must therefore be expressible as

$$\mathbf{r}_0 = \alpha \mathbf{H}_m + \beta \mathbf{H}_n + \gamma \mathbf{H}_m \times \mathbf{H}_n, \tag{6}$$

$$\hat{\mathbf{a}} = \lambda \mathbf{H}_m + \mu \mathbf{H}_n + \nu \mathbf{H}_m \times \mathbf{H}_n, \tag{7}$$

for some choice of the scalars α, β, γ, λ, μ, ν. Since eq. (3) shows that $\hat{\mathbf{a}}$ must be perpendicular to both $\mathbf{H}_m$ and $\mathbf{H}_n$, it follows that $\lambda = \mu = 0$. Choosing ν so that $\hat{\mathbf{a}}$ is a unit vector results in eq. (5) for $\hat{\mathbf{a}}$.

Turning now to eq. (6) for $\mathbf{r}_0$, note that by definition $\mathbf{r}_0$ is perpendicular to $\hat{\mathbf{a}}$ (and therefore to $\mathbf{H}_m \times \mathbf{H}_n$), so $\gamma = 0$. To find α and β, take the inner product of eq. (6) with $\mathbf{H}_m$ and $\mathbf{H}_n$ in turn. The resulting scalar equations may be solved for α and β,

$$\alpha = \frac{\mathbf{r}_0 \cdot \mathbf{H}_m H_n^2 - \mathbf{r}_0 \cdot \mathbf{H}_n \mathbf{H}_m \cdot \mathbf{H}_n}{H_m^2 H_n^2 - (\mathbf{H}_m \cdot \mathbf{H}_n)^2}, \tag{8}$$

$$\beta = \frac{\mathbf{r}_0 \cdot \mathbf{H}_n H_m^2 - \mathbf{r}_0 \cdot \mathbf{H}_m \mathbf{H}_m \cdot \mathbf{H}_n}{H_m^2 H_n^2 - (\mathbf{H}_m \cdot \mathbf{H}_n)^2} \tag{9}$$

But eq. (3) shows that $(\mathbf{r}_m - \mathbf{r}_0) \cdot \mathbf{H}_m = 0$, so that $\mathbf{r}_0 \cdot \mathbf{H}_m = \mathbf{r}_m \cdot \mathbf{H}_m$ (and similarly for n). When this identity is substituted into eqs. (8) and (9), which in turn (along with $\gamma = 0$) are substituted into eq. (6), one obtains eq. (4) for $\mathbf{r}_0$.

SCARAB's computer uses eqs. (4) and (5) as follows. For each pair of magnetometers, the computer calculates a value of $\mathbf{r}_0$ and $\hat{\mathbf{a}}$, and furthermore calculates two estimates of the cable current by twice solving eq. (3) for the current necessary to account for each of the two observed field magnitudes. Because four magnetometers can be paired in six ways, these computations provide six estimates of $\mathbf{r}_0$ and $\hat{\mathbf{a}}$ which are then averaged with the weight function,

$$w_{mn} = \frac{|\mathbf{H}_m \times \mathbf{H}_n|^4}{H_m^4 H_n^4}, \tag{10}$$

which expresses the fourth power of the sine of the angle between $\mathbf{H}_m$ and $\mathbf{H}_n$ (a choice of w_{mn} whose motivation was discussed in Section 3.4). For example,

$$\langle \mathbf{r}_0 \rangle = \frac{\sum_{i>j=1}^{4} w_{ij} \mathbf{r}_0(\mathbf{H}_i, \mathbf{H}_j, \mathbf{r}_i, \mathbf{r}_j)}{\sum_{i>j=1}^{4} w_{ij}}, \tag{11}$$

and similarly for $\hat{\mathbf{a}}$ (which, in addition, is normalized to unit magnitude). An estimated cable current is also obtained, using a similar weighted average. In all these averages, magnetometer pairs for which $\mathbf{H}_m$ and $\mathbf{H}_n$ are nearly parallel (to within one degree) are omitted to avoid the computational singularity when $\mathbf{H}_m \| \mathbf{H}_n$ [which would cause the denominators of eqs. (4) and (5) to vanish]. Also omitted are any magnetometers whose contribution SCARAB's operator wishes to exclude (e.g., a malfunctioning magnetometer).

Having thus calculated an estimated cable location, the final computation uses the heading, pitch, and roll data to transform this cable location from a coordinate system fixed in the vehicle to a coordinate system independent of vehicle orientation. The cable location is then ready to be displayed to SCARAB's operator.

5.3 Data displays

The computer calculates a new cable-location estimate about twice per second, in the manner described above, and communicates this estimate to SCARAB's operator by means of a plasma display panel. Both computer and display are located in SCARAB's operator control hut, pictured in Fig. 6. The display format shown in Fig. 7 is one of several which the operator can invoke to aid in the various phases of SCARAB's operations. The particular format of Fig. 7 shows the estimated cable location in plan view relative to SCARAB's position, with SCARAB's heading indicated both numerically and by the orientation of the vehicle symbol (whose rectangular outline is drawn to scale to represent the actual location of the vehicle's perimeter). The estimated cable current and the operator-selected averaging time are also displayed.

When the vehicle is far from the cable, the magnetic data are dominated by noise and the cable-location estimates are random and meaningless. To suppress such estimates, the computer examines the cable-location estimates to establish their credibility before displaying them. For example, a cable-location estimate is not displayed if it is blatantly inconsistent with the preceding estimate. The criteria for credibility are sufficient to identify most estimates that are dominated by noise, so that in the absence of a cable the operator is not distracted by a random succession of meaningless lines.

A variation of this display format, shown in Fig. 8, includes a history of the estimated burial depth of the cable. This estimate is determined by subtracting SCARAB's height above the bottom (as measured by its altimeter) from its estimated height above the cable (given by the vertical component of $\mathbf{r}_0$, appropriately adjusted if a nonhorizontal $\hat{\mathbf{a}}$ indicates a sloping sea bottom). The estimated burial depth is more severely affected by noise than the estimated cable location, because the former is the difference between two larger quantities, each subject to noise. Accordingly, provision has been made for the burial depth to be time-averaged, with its averaging time chosen by the operator. This averaging time can be chosen substantially longer than the averaging time for the raw data, because at slow vehicle speeds the actual burial depth changes quite slowly with time.

A third display format (Fig. 9) shows a history of the three magnetic-field components measured by a single magnetometer (selected by the operator). This display is useful for troubleshooting, since the effects of a malfunctioning magnetometer are immediately apparent. It is also useful for cable detection when SCARAB is more than a few meters away from the cable (i.e., outside the cable-localization range but inside the cable-detection range). Furthermore, in cases when the signal is so weak that the cable-localization algorithm is ineffective at

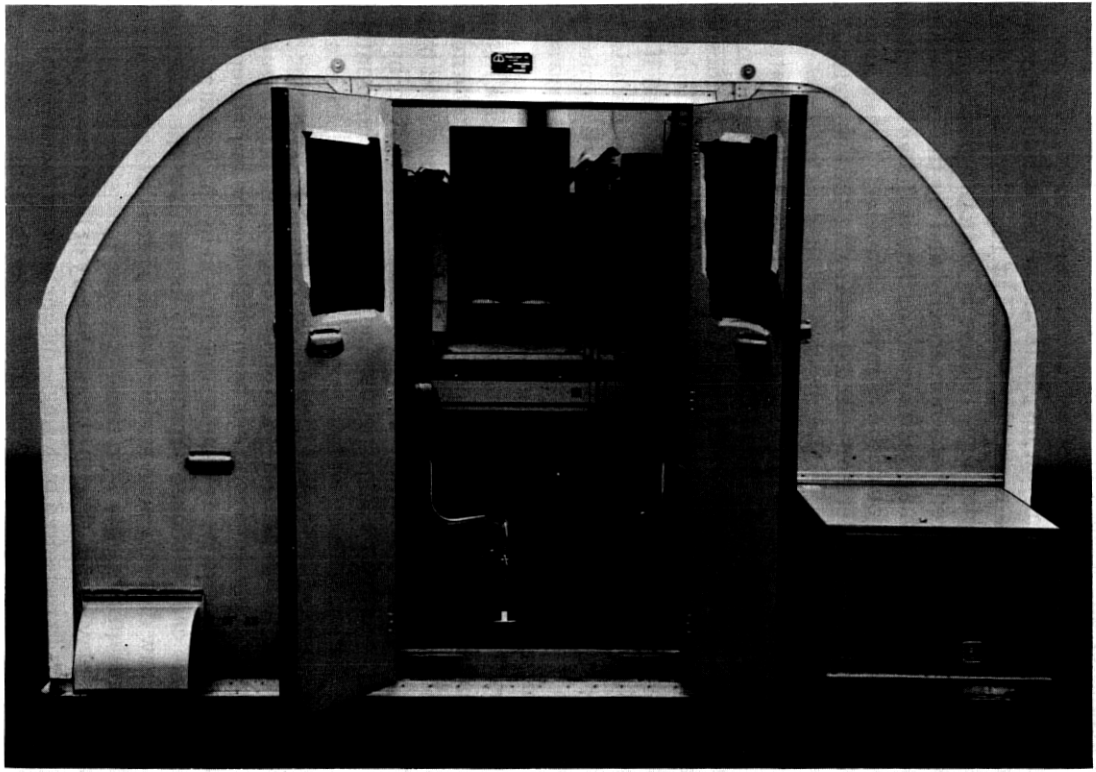

Fig. 6—SCARAB operator control hut. Computer keyboard and display are partially obscured but visible at the right-hand seat.

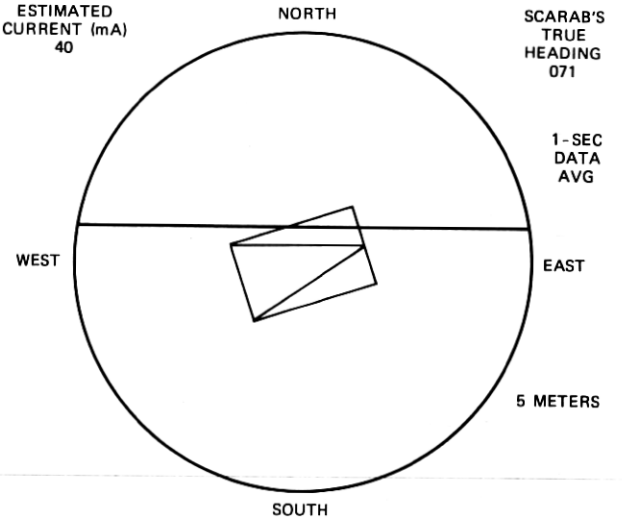

Fig. 7—Real-time computer display showing estimated cable location relative to SCARAB, in plan view.

any range, cable tracking using this display may still be possible, as described in the next section.

VI. OPERATIONAL USE OF THE SYSTEM

At the time of this writing, sea trials of the cable-locating system have been completed. The first tests were done by emplacing a length

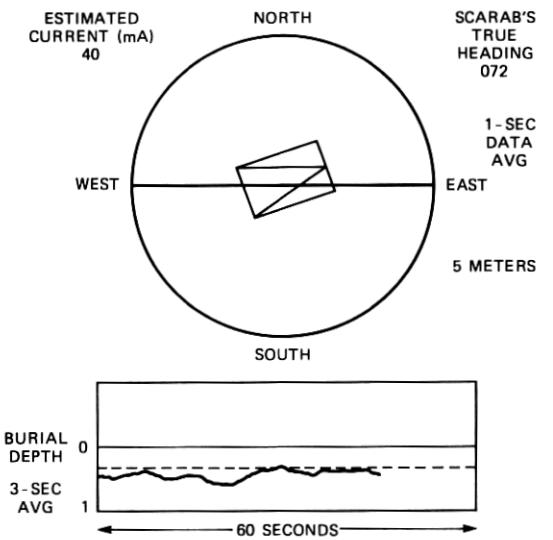

Fig. 8—Real-time computer display showing estimated cable location and a short history of estimated burial depth.

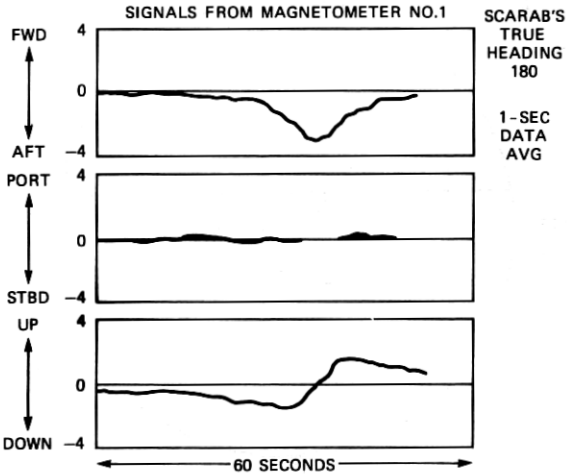

Fig. 9—Real-time computer display showing the three components measured by a magnetometer as a function of time.

of trial cable, applying a 25-Hz tone, and then acquiring and tracking the cable using the system. Later, tests were done on two operational cable systems. Finally, the system was used during the burial of a section of an operational cable.

Background noise levels were noted under various conditions throughout the trials. During vehicle pre-dive checkouts, noise levels were noted with the vehicle on deck. In this situation, magnetometer outputs were noted to vary randomly in the range of $\pm 0.3\gamma$. After the vehicle was launched it maneuvered on the surface for some time without using vertical thrusters and the outputs would decrease to $\pm 0.2\gamma$. At the beginning of a dive, the outputs increased to as much as several gammas. These levels result from the 25-Hz field components emitted from the vertical thrusters as they pass through the speed at which their slip frequency is 25 Hz. These noise levels were evident many times during descent as the vertical thruster levels were varied by the operators.

When the vehicle reached the bottom, vertical thrust was increased to 100 percent and magnetometer levels subsided to less than $\pm 0.5\gamma$. Transients of about 2γ were observed on all channels whenever vehicle lights were turned on (or off).

The location of the dive was generally far enough from the trial cable so that acquisition would be initiated by dead reckoning. As the vehicle approached the estimated cable position, a numerical display of magnetometer signals was observed to monitor the vertical fields measured by the magnetometers. (As an alternative, the vertical field of a single magnetometer could be observed in a time series using the

display of Fig. 8.) When an appreciable vertical field was observed, the display of Fig. 6 was used to allow the vehicle operator to track the cable.

When a specially laid trial cable was used an initial tone current of 200 mA (rms) was used. Field levels as large as 22γ were indicated and the cable was successfully tracked at an altitude of 4 meters.

After some confidence was established, tone current was reduced to 100 mA and then to 50 mA and indications were not noticeably degraded. Further reduction of the current to 10 mA (rms) produced an objectionable disturbance in the display, but it was still useful. There is some evidence that the actual cable currents may have been somewhat smaller than these values, because of injection losses where the current was applied to the cable; this effect was not quantified.

The burial-depth feature gave somewhat inaccurate results when the vehicle was maneuvering off the bottom, because of fluctuating altimeter readouts; however, stable and repeatable results were obtained when the vehicle was held on the bottom by its thrusters. In this mode of operation, the operator notifies the computer that SCARAB is being held on the bottom, and the computer therefore ignores the altimeter in determining burial depth. Thus, any inaccuracy in the altimeter is avoided. In addition, maneuver noise is reduced and vertical thruster levels tend to remain above the range in which 25 Hz emission occurs.

During the trials on operational cables, SCARAB was operated about 100 nmi from the cable terminal where the tone was applied to the cable. Tone currents of 20 and 30 mA (rms) were used. As a result, the actual 25-Hz current at the point of operation was only about 5 mA (rms). This proved marginal. Cable acquisition with the vehicle at an altitude of one meter could not be accomplished using the magmetometer system; however, after the cable was acquired visually, tracking was possible. The system indicated an estimated tone of 3–6 mA during these tests. It should be remembered that during acquisition and tracking of faulted cables (SCARAB's principal mission), current levels can be used which are an order of magnitude higher than these.

The system was later used during the burial of an operational cable. Here, the indicated tone current was 10 mA and both acquisition and tracking were possible.

In view of the brevity of these trials, a full evaluation of the capabilities and limitations of the system must await actual operations. However, since the sea trials tended to confirm performance predictions, it seems likely that the system's performance is well enough known to support the following speculations as to the likely operational use of the system during a cable-repair operation.

With SCARAB on board, the cable-repair ship will steam to the estimated fault location and, perhaps with the aid of towed electrodes

or induction coils to sense the 25-Hz tone, will position itself shoreward of the fault and relatively near the known cable track (though not so near that the direction to the cable is ambiguous). After launch, SCARAB will proceed on or close to the seabed at a speed of about 1 knot in a direction that will cross the cable at right angles, with SCARAB's crew monitoring the computer display of Fig. 9 to watch for the cable's presence.

At a few tens of meters from the cable, its signal will start to rise out of the noise. As the cable is crossed, the characteristic signature shown in Fig. 9 will be observed, indicating that the cable has been crossed. SCARAB's operator will then turn the vehicle back toward the cable, intercepting it obliquely and then swimming directly above it toward the fault, using the display of Fig. 7 to facilitate cable tracking. Except in severe ocean currents, SCARAB should be able to stay within a few meters of the cable, so the restricted range of the localization algorithm should pose no handicap. Gentle bends in the cable should not affect the tracking algorithm adversely, as long as their radius of curvature is large compared with the dimensions of the magnetometer array. Sharper bends normally will be unburied, therefore causing no confusion if visibility is adequate. If the cable current is less than about 10 mA (rms), it may be insufficient for tracking using the tracking algorithm. However, SCARAB may still be able to track the cable using the display of Fig. 9, either by steering so as to maintain a zero vertical field component or by zigzagging across the cable, ascertaining from the display each time the cable is crossed.

When the cable fault is reached, it may very well be recognizable visually, either because the cable was pulled out of the bottom when it was broken or because the source of the damage (e.g., a trawler's otter boards) left visible tracks in the bottom. If there is no visual indication, the fault location may be recognized by the sudden decrease in the magnetic field, causing a deterioration of the cable-location estimate as the fault location is passed, accompanied by a sudden decrease in the estimated cable current. This effect results from the nature of the field near the end of the cable, where the field magnitude falls to zero in a horizontal distance comparable to the vertical distance of the vehicle above the cable. SCARAB's cable-location estimate will therefore deteriorate completely in a distance of about a meter (corresponding to an elapsed time of about 2 s at a speed of 1 knot), showing that the fault has been passed. With this realization, SCARAB's operator can circle back, reacquire the cable, and position SCARAB on the bottom near the fault, perhaps recognizing the precise fault location by the fact that when SCARAB is directly over the fault the magnetic field (and hence the estimated cable current) will have fallen to half the value it had before the area of the fault was reached. Once SCARAB

is on the bottom at the fault, it will use its dredger to unbury the cable, and the job of the cable-localization system is complete.

VII. SUMMARY

Increasing reliance on burial to protect undersea cable has led to the construction of the SCARAB submersible, whose ability to find and track such cable is clearly crucial to its success. SCARAB's primary cable-finding system is similar to previous ship-based cable-finding systems in that it requires a 25-Hz tone on the cable, but it is considerably more sophisticated than these previous systems so that the cable-tracking job is made as easy as possible. A ship-based minicomputer processes signals from four three-axis magnetometers aboard the vehicle, estimating the relative cable location, and displaying it pictorially to SCARAB's operator. The principal difficulties encountered in implementing the system were caused by two types of noise source on the vehicle: the thruster motors, and currents induced in SCARAB's framework by the cable's 25-Hz field. The thruster noise was circumvented by placing the magnetometers as far as possible from the thrusters and avoiding the thruster speed which would result in noise concentrated at 25 Hz. The frame-current problem was reduced to acceptable levels by inserting insulating splices in the frame members nearest the magnetometers, after mounting the magnetometers at locations where frame members were relatively sparse. Once these problems were overcome, the system was found to function satisfactorily with cable currents down to about 10 mA (rms). So far, operational use has been rather limited, and the outer limits of the system's performance have not yet been defined. Nevertheless, it seems clear that the system does provide SCARAB with the necessary capability for finding and tracking buried cable.

VIII. ACKNOWLEDGMENTS

The authors wish to thank J. C. Wyman for his valuable technical contributions to the project, and N. J. Zabusky for his guidance and support during the project's formative phases. We are also indebted to the crew of CURV III and the AT&T cableship C.S. Long Lines and to the personnel of the Franklin Electric Company for their cooperation in the use of their facilities.

APPENDIX

Low-Frequency Propagation on Undersea Coaxial-Cable Systems

This appendix concerns the propagation on undersea coaxial-cable systems of signals whose frequency is sufficiently low that the electromagnetic fields are not confined to the cable but penetrate substan-

tially into the sea water. The purpose of the analysis is to calculate the signal levels in the neighborhood of the cable as a function of distance offshore, so that the performance of SCARAB's cable-locating system can be predicted. The analysis includes the effects of the repeaters, which have an important influence on signal attenuation.

In practice, an upper limit on the achievable signal level is given by the maximum low-frequency current tolerated by the repeaters. This maximum is 200 mA (rms) in the most recently installed system (the SG system), but is 100 mA (rms) on earlier systems. When in service, all systems require that the low-frequency signal be kept below 20 mA (rms). These maxima refer to the center-conductor current inserted at the shore termination; signal losses in the cable and repeaters govern how much of this signal actually reaches the point of interest (i.e., SCARAB's location), and shielding by the cable's outer conductor and armor wires determines how much of this center-conductor current can be seen by SCARAB's sensors.

The analysis of this problem divides naturally into two stages: a waveguide analysis using Maxwell's equations to determine the properties of the propagating modes, and a transmission-line analysis using these mode properties to study signal propagation on a repeatered cable system. The principal idealizations of the analysis, necessary to preserve the cylindrical symmetry of the waveguide problem, are twofold. The electromagnetic properties of the sea bottom are taken to be identical with those of sea water (insofar as they affect propagation on the cable), and the effects of armor wires (if present) are assumed the same as the effects of a cylindrical shell of equal conducting cross section. Both assumptions are plausible, but no detailed justification of either is attempted. (The theoretical analysis of coaxial cables with helically wound wire shields has recently begun to receive attention,[4] but only in the limit of infinitely thin wires, which is an inappropriate limit for the problem at hand because the diameter of the armor wires exceeds the skin depth at the frequencies of interest.)

A.1 WAVEGUIDE ANALYSIS: THE PROPAGATING MODES

The electromagnetic fields propagating along a cable are governed by Maxwell's equations which, when expressed in cylindrical coordinates (ρ, ϕ, z), become

$$\frac{1}{\rho}\frac{\partial}{\partial \rho}\rho H_\phi = \epsilon' j\omega E_z, \tag{12}$$

$$-jk_z E_\rho - \frac{\partial E_z}{\partial \rho} = -j\omega\mu H_\phi, \tag{13}$$

$$jk_z H_\phi = \epsilon' j\omega E_\rho, \tag{14}$$

where the field dependence on time t and longitudinal distance z is assumed to be $\exp(j\omega t - jk_z z)$, all fields are taken to be independent of the azimuthal angle ϕ, and

$$\epsilon' = \epsilon + \sigma/j\omega. \tag{15}$$

The constitutive parameters are the conductivity σ, the permeability μ, and the permittivity ϵ.

Equations (12) through (14) relate the three field components H_ϕ, E_ρ, and E_z which comprise cylindrically symmetric TM modes. A similar set of equations (not shown) relates the components E_ϕ, H_ρ, and H_z for cylindrically symmetric TE modes. TM and TE modes without cylindrical symmetry also exist. However, the cylindrically symmetric TM modes are the only propagating modes at the low frequencies of interest here, and the other modes are neglected.

Eliminating the electric fields from eqs. (12) through (14) yields the following equation for H_ϕ:

$$\left(\frac{\partial}{\partial\rho}\frac{1}{\rho}\frac{\partial}{\partial\rho}\rho + k_\rho^2\right)H_\phi = 0, \tag{16}$$

where

$$k_\rho = (\omega^2\epsilon'\mu - k_z^2)^{1/2} \quad \mathrm{Im}(k_\rho) > 0. \tag{17}$$

The general solution of eq. (16),

$$H_\phi = AJ_1(k_\rho\rho) + BY_1(k_\rho\rho), \tag{18}$$

involves the Bessel functions J_1 and Y_1 and the arbitrary constants A and B. E_z can be derived from eqs. (12) and (18),

$$E_z = \frac{k_\rho}{\epsilon' j\omega}[AJ_0(k_\rho\rho) + BY_0(k_\rho\rho)]. \tag{19}$$

Coaxial cable consists of a number (N) of homogeneous cylindrical layers in which the electromagnetic fields take the form given by eqs. (18), (19), and (14) with A, B, k_ρ, and ϵ' assuming different values in each layer. The constants A and B in each of the N layers are constrained to satisfy the $2(N-1)$ boundary conditions of continuous H_ϕ and E_z at the $N-1$ cylindrical interfaces. Furthermore, the requirement that the solution be finite at $\rho = 0$ and $\rho = \infty$ implies that $B = 0$ in the central region and $B = jA$ in the outermost layer. These $2N$ constraints imply $2N$ linear equations that the $2N$ amplitudes A and B must satisfy. To permit a solution, k_z must be chosen so that the determinant of the $2N \times 2N$ matrix of coefficients vanishes.

It is easy to show that the number of such eigenvalues k_z corresponding to propagating modes equals the number of insulating layers. If the conductors (including the sea water) are perfect, this equality is

clear, for electromagnetic waves can propagate in each insulating layer independently, each such layer therefore supporting its own single propagating TEM mode. In this limit, the coaxial cable comprises a number of parallel and independent waveguides isolated from one another by perfectly conducting walls. If the conducting layers have finite conductivity, however, the waveguides are no longer independent, since electromagnetic waves can penetrate the conductors, but the number of modes remains the same. In this case the modes overlap spatially but differ from one another in their relative distribution of energy among the various insulating layers as well as in their longitudinal wave number k_z.

To illustrate the nature of these modes, we modeled a particular cable type (SG cable) and solved the eigenvalue problem. Unarmored SG cable comprises a central steel strength member (1.06 cm o.d.), a copper inner conductor (1.21 cm o.d.), a dielectric (4.32 cm o.d.), a copper outer conductor (4.37 cm o.d.), and a protective jacket (5.28 cm o.d.). For these calculations, the conductivities of copper, steel, and sea water are taken to be 5.9×10^7, 4.8×10^6, and 4 mhos/m, respectively, the permittivities of the insulators are $2.285\epsilon_0$ (where ϵ_0 is the permittivity of free space), the permittivity of sea water is $81\ \epsilon_0$, and the permeability of steel is $180\ \mu_0$ (with μ_0 the permeability of free space).

Figure 10 shows the field distributions corresponding to the two propagating modes of unarmored SG cable at 25 Hz. Mode 1 is the generalization of the TEM mode which, if the conductors were perfect, would be confined between the inner and outer conductors, while mode 2 is the generalization of the TEM mode which would be confined between the outer conductor and the sea. The attenuation lengths (defined as $-1/\mathrm{Im}[k_z]$) of these modes are 330 nautical miles and 115 nautical miles at 25 Hz. At neighboring frequencies, the attenuation lengths scale roughly as the inverse square root of the frequency.

A.2 TRANSMISSION-LINE ANALYSIS

To predict signal propagation on a cable with N conductors (where $N = 2$ for unarmored cable and $N = 3$ for single-armored cable), we must calculate the appropriate amplitudes of the $2N$ modes (N types of modes, two directions of propagation) on each repeater section. The superposition of these modes must satisfy the relevant boundary conditions (expressed as constraints on voltages and currents) at each end of the section. This analysis requires an equivalent circuit for the repeaters, which is shown in Fig. 11.[5] The repeater's equivalent impedance depends strongly on whether dc power is applied (as indicated in Fig. 11). The cable's outer conductor and armor wires (if present) are grounded to sea at each repeater, as shown.

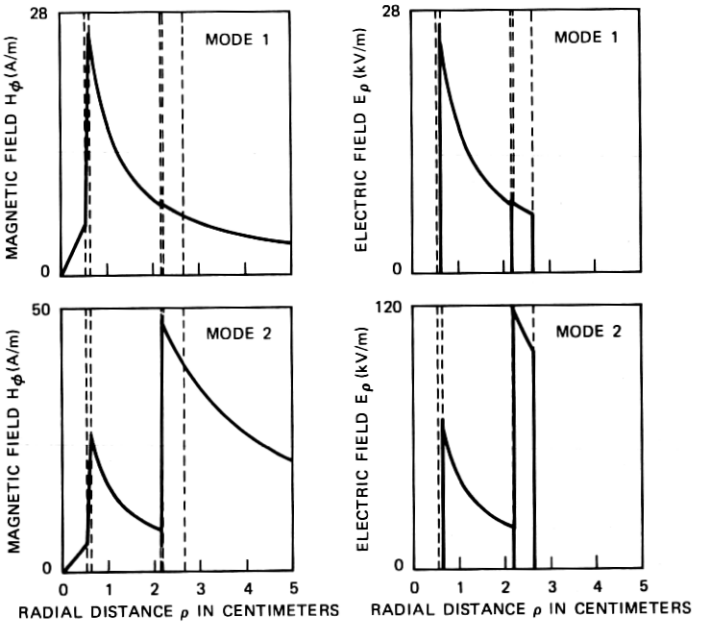

Fig. 10—Field amplitudes of the two propagation modes of unarmored SG cable at 25 Hz. The broken lines indicate the boundaries of the cable's layers: central strength member, inner conductor, dielectric, outer conductor, outer jacket, and sea water.

The transmission-line analysis is largely an exercise in matrix manipulation, and its details (which involve considerable notational complexity) will not be given in the interests of brevity. The procedure starts at the offshore cable break, where all N conductors are grounded to sea. These N constraints on the mode amplitudes, along with the $N - 1$ constraints that all conductors except the center conductor are

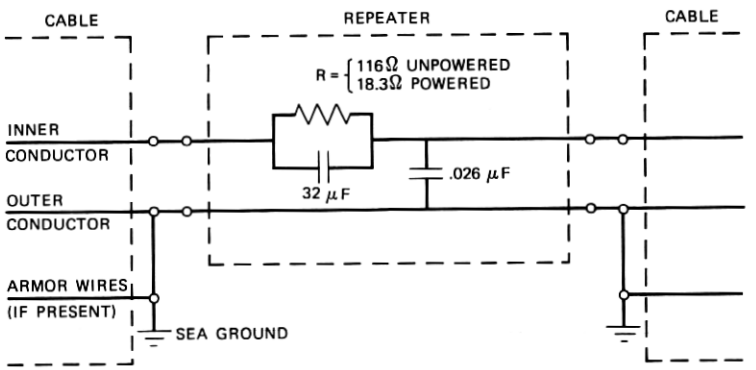

Fig. 11—Equivalent circuit of SG repeater at low frequencies. The equivalent resistance R is 18.3Ω if dc power is applied to the repeater, 116Ω otherwise.

grounded to sea at the offshore end of the most offshore repeater, provide $2N - 1$ constraints on the $2N$ modes propagating in the last cable section (i.e., the one between the last repeater and the cable break). The relative amplitudes of these modes can therefore be determined, leaving only an arbitrary multiplicative constant (common to all the modes) to be adjusted later. These mode amplitudes can be manipulated to provide the voltage and current at the offshore port of the last repeater, and conventional circuit analysis then provides the voltage and current at the shoreward port. These values of the voltage and current provide two constraints on the $2N$ modes in the next shoreward cable section, with the other $2N - 2$ constraints coming from the fact that all conductors but one (the center conductor) are grounded to sea at both ends of the cable section. The $2N$ mode amplitudes in the next-to-last cable section can therefore be found.

In this way, the solution is propagated from the cable break back toward the shore terminal, with the mode amplitudes being determined in each cable section so that the appropriate constraints on voltages and currents are satisfied at the cable break and at both ports of every repeater. Once the solution is complete, it is adjusted by a multiplicative constant so as to satisfy the driving-point condition (e.g., that the center-conductor current be 200 mA at the shore terminal).

Figure 12 shows the results of such a calculation, and assumes a

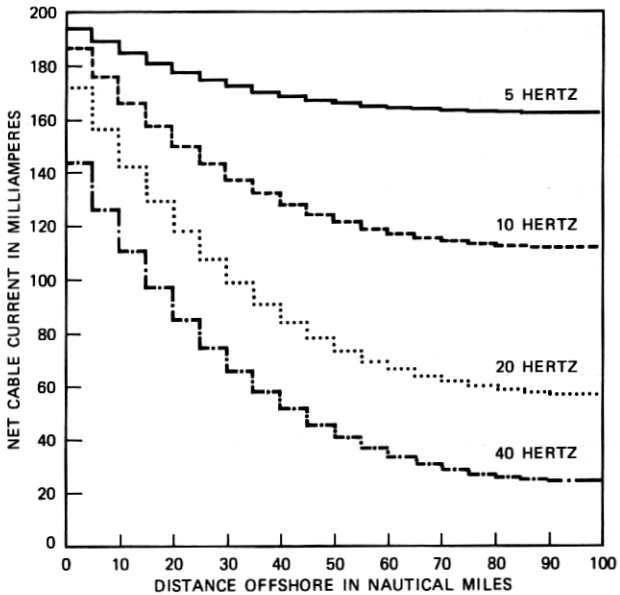

Fig. 12—Propagation of low-frequency signals on unarmored SG cable with a cable break 100 nmi offshore. The center-conductor current is 200 mA at the shore point, for all frequencies. The step discontinuities occur at the repeaters, which are unpowered.

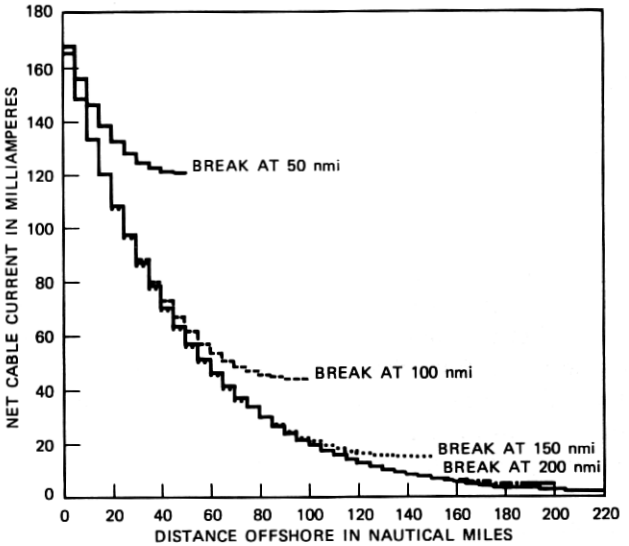

Fig. 13—Propagation of 25-Hz signals on unarmored SG cable, with cable breaks at various locations. The unlabeled curve extending to 220 nmi is for a cable with no break. The center-conductor current is 200 mA at the shore point. The step discontinuities occur at the repeaters, which are unpowered.

cable break to be 100 miles offshore. The repeaters are spaced at 5-mile intervals, and their presence is evident by the step discontinuities in the net cable current, which is defined as the algebraic sum of all currents on the cable's conductors. The step discontinuities are caused by the exchange of current between the outer conductor and the sea at each repeater. The center-conductor current itself (not shown) decays smoothly with distance, without appreciable step discontinuities, because the repeaters provide no low-impedance path from the center conductor to sea. The center-conductor current is 200 mA at the shore point in Fig. 12, but the net current is somewhat less because of the return current carried by the outer conductor. This outer-conductor current increases with frequency, so that the net current decreases with frequency.

Just as Fig. 12 illustrates the frequency dependence of the signal propagation, Fig. 13 illustrates the dependence on the distance to the cable break at SCARAB's chosen frequency of 25 Hz. One predominant feature of Fig. 13 is that the cable break reflects the propagating modes, doubling the signal amplitude relative to its value in the absence of a break. Another important conclusion supported by Fig. 13 is that the signal losses are primarily introduced by the repeaters, rather than by losses in the cable. This conclusion is borne out by the fact that the decay from 165 mA at the shore point to 1.7 mA at 220

nmi corresponds to an attenuation length of about 50 nmi, much less than the 330-nmi attenuation length of the cable's primary mode. Since the repeaters account for most of the signal attenuation (at least at 25 Hz), it follows that an improvement in propagation would result from a reduction in the repeater's impedance at 25 Hz. Because powering the repeaters reduces their impedance considerably (as Fig. 11 points out), 25-Hz propagation on a powered system (illustrated in Fig. 14) is much less attenuated than on an unpowered system. For example, the signal at 200 nmi is increased by more than a factor of 10 when the system is powered, as comparison of Figs. 13 and 14 reveals. Substantial further improvement in 25-Hz propagation on future cable systems would result from the inclusion of a bypass network allowing the 25-Hz signal to pass through the repeaters unattenuated. Such an improvement would increase the usefulness of SCARAB's cable-localization system by allowing useful signal levels to propagate farther offshore.

The calculations in this appendix so far have dealt with unarmored cable. Since many existing cable systems (and probably all future cable systems) employ armored cable on the continental shelves, it is of interest to see how armored and unarmored cable differ in their propagation characteristics. To this end, calculations involving armored cable have been carried out, modeling single-armored SG cable as identical to unarmored SG cable with the addition of a steel armor layer (6.3 cm o.d.) sandwiched between two jacket layers (5.75 and 6.76

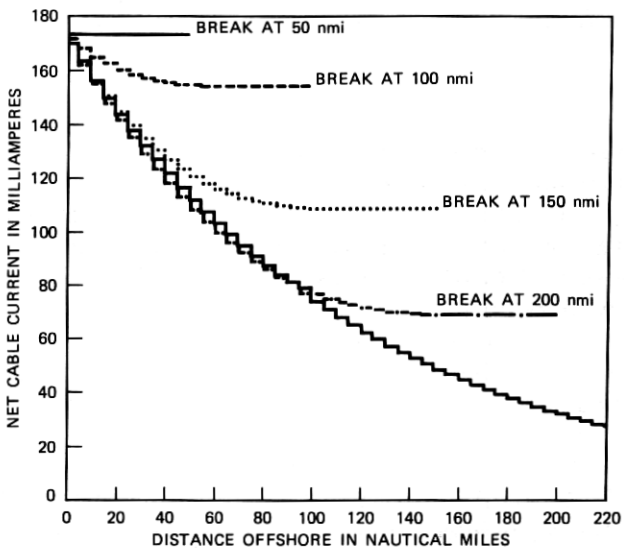

Fig. 14—Same as Fig. 13 except that the repeaters are powered, which reduces their impedance at 25 Hz.

cm o.d.). The three propagation modes of armored cable have attenuation distances at 25 Hz of 260, 140, and 86 nmi (compared with 330 and 115 nmi for unarmored cable). Propagation on armored cable at various frequencies is illustrated in Fig. 3, and propagation at 25 Hz with cable breaks at various locations is illustrated in Fig. 4. Comparison of Figs. 3 and 4 with their counterparts for unarmored cable (Figs. 12 and 13) shows one outstanding difference: the net current on the armored cable is reduced by the shielding effect of the armor layer (which carries a substantial amount of return current, particularly at the higher frequencies). At 25 Hz, for example, the net current on armored cable is only about 40 percent of that on unarmored cable. This ratio is about equal to the quantity $\exp(-\Delta\rho/\delta)$, where $\Delta\rho$ is the thickness of the armor layer and $\delta = (2/\omega\mu\sigma)^{1/2}$ is the skin depth in steel (which is a better shield even than copper because of its high permeability μ, which more than compensates for its lower conductivity σ). The attenuation of the signal with distance offshore, being governed primarily by the repeaters rather than the cable, is the same for both armored and unarmored cable.

A.3 SUMMARY

This appendix has presented the results of theoretical calculations of propagation on SG repeatered cable systems (both armored and unarmored). Propagation at various frequencies, with cable breaks at various locations, and with both powered and unpowered repeaters, is displayed in Figs. 3, 4, 12, 13, and 14. These figures show that, if 10 mA (rms) is taken as the necessary current level for cable localization by SCARAB, and if 200 mA (rms) of 25-Hz center-conductor current is applied at the shore terminal of an unpowered unarmored SG system, then breaks as far offshore as 170 nmi can be found (with this value reduced to 125 nmi for armored cable, because of the shielding effect of the armor wires). These ranges can be increased if dc power can be applied to the repeaters, thereby reducing their impedance. If less current is applied at the shore point (as on earlier cable systems, which can tolerate only 100 mA, or on operational systems, which can tolerate only 20 mA), the maximum effective range of SCARAB's cable-locating system is correspondingly reduced.

These operational ranges could be increased for future cable systems by designing the repeaters with a separate low-impedance path for the 25-Hz signal to avoid the constraints and losses imposed on this signal as it traverses the dc power path.

REFERENCES

1. H. A. Baxter and R. E. Mueser, "The Development of Ocean-Cable Plows," IEEE Trans. Commun. Technol., *COM-19*, No. 6 (December 1971), pp. 1233–41.

2. G. S. Cobb, "Sea Plow IV—An Underseas Vehicle for Burying Ocean Cable," in *OCEANS '76*, New York: Institute of Electrical and Electronics Engineers, 1976, pp. 19B-1 to 19B-6.
3. G. R. Barnard, Applied Research Laboratory, University of Texas, Austin, Texas, personal communication, 1975.
4. J. R. Wait, "Electromagnetic Theory of the Loosely Braided Coaxial Cable: Part I," IEEE Trans. Microwave Theory Technol., *MTT-24*, No. 9 (September 1976), pp. 547–53.
5. C. D. Anderson, Bell Laboratories, Holmdel, New Jersey, personal communication, 1977.